

Highly Improved Electroluminescence from a Series of Novel Eu^{III} Complexes with Functional Single-Coordinate Phosphine Oxide Ligands: Tuning the Intramolecular Energy Transfer, Morphology, and Carrier Injection Ability of the Complexes

Hui Xu,^[b] Kun Yin,^[c] and Wei Huang*^[a]

Abstract: The functional single-coordinate phosphine oxide ligands (4-diphenylaminophenyl)diphenylphosphine oxide (TAPO), (4-naphthalen-1-yl-phenylaminophenyl)diphenylphosphine oxide (NaDAPO), and 9-[4-(diphenylphosphinoyl)phenyl]-9*H*-carbazole (CPPO), as the direct combinations of hole-transporting moieties, and electron-transporting triphenylphosphine oxide (TPPO) were designed and synthesized (amines or carbazole), together with their Eu^{III} complexes [Eu(tapo)₂(tta)₃] (**1**), [Eu(nadapo)₂(tta)₃] (**2**), and [Eu(cppo)₂(tta)₃] (**3**; TTA: 2-thenoyltrifluoroacetate). The investigation indicated that by taking advantage of the modification inertia of the phosphine oxide ligands, the direct in-

roduction of the hole-transport groups as chromophore made TAPO, NaDAPO, and CPPO obtain the most compact structure and mezzo S₁ and T₁ energy levels, which improved the intramolecular energy transfer in their Eu^{III} complexes. The amorphous phase of **1–3** proved the weak intermolecular interaction, which resulted in extraordinarily low self-quenching of the complexes. The excellent double-carrier transport ability of the ligands was studied with Gaussian calculations, and the bipolar structure of TAPO and

CPPO was proved. The great improvement of the double-carrier transport ability of **1–3** was shown by cyclic voltammetry. Their HOMO and LUMO energy levels of around 5.3 and 3.0 eV, respectively, are the best results for Eu^{III} complexes reported so far. A single-layer organic light-emitting diode of **2** had the impressive brightness of 59 cd m⁻² which, to the best of our knowledge, is the highest reported so far. Both of the four-layer devices based on pure **1** and **2** had a maximum brightness of more than 1000 cd m⁻², turn-on voltages lower than 5 V, maximum external quantum yields of more than 3% and excellent spectral stability.

Keywords: electroluminescence • europium • hole transport • ligand design • P ligands

Introduction

For decades, lanthanide complexes have been studied as emitters in organic light-emitting diodes (OLEDs) with the advantages of a nearly monochromatic characteristic emission, chemical environmental stability, and approaching 100% theoretical internal device quantum efficiency.^[1–8] However, for many reasons the electroluminescence (EL) performance of these lanthanide materials is still much lower than what people expect. The unbalanced hole and electron injection and transport should be one of the most important factors. In most lanthanide complexes, the materials tend to transport electrons rather than holes.^[1] Therefore, much work was done to improve the hole-transport ability of the lanthanide complexes through modification with hole-transport moieties. Hole-transport moieties, such as *N*-ethylcar-

[a] Prof. W. Huang
Institute of Advanced Materials (IAM)
Jiangsu Key Laboratory of Organic Electronics
and Flat-Panel Displays
Nanjing University of Posts and Telecommunications (NUPT)
66 XinMoFan Road, Nanjing 21003 (China)
Fax: (+86)25-8349-2333
E-mail: wei-huang@njupt.edu.cn

[b] Dr. H. Xu
School of Chemistry and Materials
Heilongjiang University (HLJU)
74 Xuefu Road, Harbin 150080 (China)

[c] K. Yin
Institute of Advanced Materials (IAM)
Fudan University
220 Handan Road, Shanghai 200433 (China)

bazolyl, were introduced into the β -diketone ligand.^[9] Furthermore, since the most popular neutral ligands, such as 1,10-phenanthroline (phen), triphenylphosphine oxide (TPPO) and 2,2'-bipyridine (bpy), also only exhibit very good electron-transport ability,^[10,11] the hole-transporting triphenylamine and carbazole groups were introduced into phen or bpy derivatives to obtain a double-carrier transport ability.^[12–15] Thus, the EL performance of these complexes was much improved.

The effect of these modifications was inspiring. However, because the lone electron pair of the N atom in phen and bpy is involved in the whole conjugated system, the introduction of the modifying groups would influence the distribution of the electron cloud of the whole nitrogen heterocyclic ring and further influence the coordination ability of the ligands. To avoid reducing the coordination ability of these phen or bpy derivatives, buffer groups were introduced between the hole-transport moieties and the coordination moieties. However, the introduction of the buffer groups made the synthetic routines much more complicated. Notably, the EL efficiencies of the OLEDs based on these complexes were not as high as expected. The intramolecular energy-transfer process in Eu^{III} complexes follows the Dexter mechanism,^[16,17] and thus the introduction of the buffer groups increased the volume of these ligands, lengthened the distance between the ligands and Eu^{III} ions, reduced the overlap of their electron clouds and as a result decreased the efficiency of the intramolecular energy transfer. So it is attractive and significant to design and synthesize highly efficient electroluminescent Eu^{III} complexes with multifunctional neutral ligands with good double-carrier transport ability and compact structure.

Tppo has been used as the neutral ligand in electroluminescent Tb^{III} complexes. The best electroluminescent Tb^{III} complex $[\text{Tb}(\text{ebpmp})_3(\text{tppo})]$ (EBPMP: 1-phenyl-3-methyl-4-(2-ethylbutyryl)-5-pyrazolone) reported so far used TPPO as the neutral ligand.^[18] Compared with phen derivatives, TPPO exhibits good electron-transport ability and strong coordination ability. However, when using TPPO in Eu^{III} complexes, their EL performance, such as brightness and efficiency of the corresponding OLED devices, was very limited.^[19] The most important factor is that the first singlet excited energy level (S_1) of TPPO is much higher than that of anionic ligands, such as 2-thenoyltrifluoroacetate (TTA). The energy gap of about 1.5 eV between them is too large to decrease the energy-transfer efficiency from TPPO to TTA. Also, the electron-transporting TPPO could not afford balanceable carrier injection and transport, which is another important reason for the low EL efficiency.

Recently, we reported the novel Eu^{III} complex $[\text{Eu}(\text{dpepo})(\text{tta})_3]$ containing the chelate phosphine oxide ligand bis[2-(diphenylphosphino)phenyl] ether oxide (dpepo).^[20] As a result of the larger conjugate area of dpepo, the energy gap between S_1 levels of dpepo and TTA was reduced to 0.8 eV. The photoluminescence (PL) and EL performance of $[\text{Eu}(\text{dpepo})(\text{tta})_3]$ was much better than that of $[\text{Eu}(\text{tppo})_2(\text{tta})_3]$. Significantly, it was proved that the direct modifica-

tion of the phosphine oxide ligand did not influence its coordination ability.

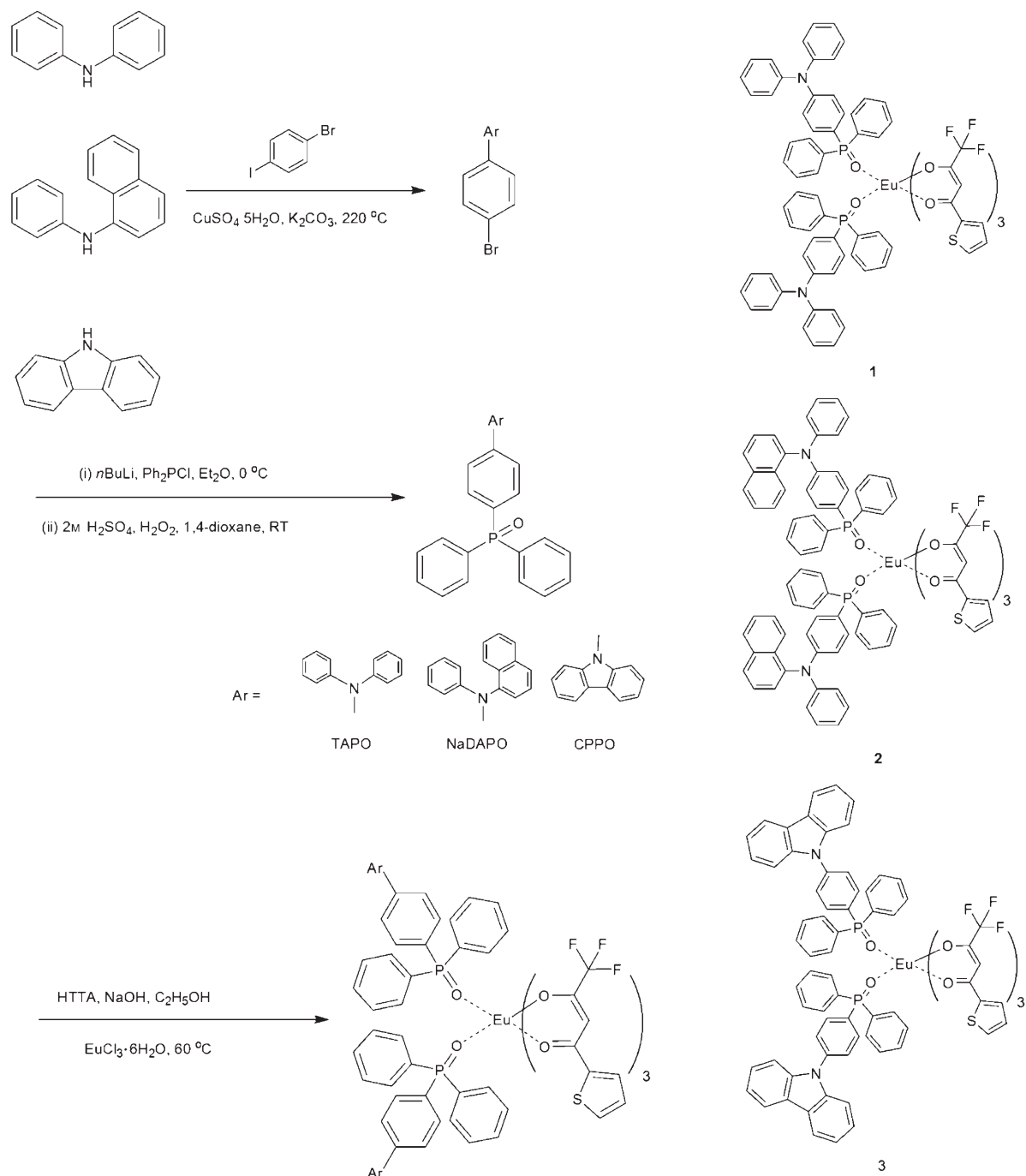
In this work, we designed and prepared (4-diphenylaminophenyl)diphenylphosphine oxide (TAPO), (4-naphthalen-1-yl-phenylaminophenyl)diphenylphosphine oxide (NaDAPO) and 9-[4-(diphenylphosphino)phenyl]-9H-carbazole (CPPO) as neutral ligands. The tertiary complexes $[\text{Eu}(\text{tapo})_2(\text{tta})_3]$ (**1**), $[\text{Eu}(\text{nadapo})_2(\text{tta})_3]$ (**2**), and $[\text{Eu}(\text{cppo})_2(\text{tta})_3]$ (**3**) based on these functional single-coordinate phosphine oxide ligands were also prepared (see Scheme 1). By taking advantage of the modification inertia of the phosphine oxide ligands, these functional ligands were designed as the direct combinations of hole-transporting moieties (diphenylamine, naphthalenyl phenylamine and carbazole), and electron-transporting TPPO to obtain double-carrier transport ability without reducing the intramolecular energy transfer. The compact structure of these ligands is helpful in making the intramolecular energy transfer more direct and efficient.

Compared with $[\text{Eu}(\text{tppo})_2(\text{tta})_3]$ complexes, **1–3** have a much better PL performance. The improvement mechanism of intramolecular energy transfer by TAPO, NaDAPO, and CPPO was suggested by measuring their excited energy levels. We studied the frontier orbital energy levels of the functional ligands and complexes **1–3** by Gaussian calculations and cyclic voltammetry (CV), respectively. It was shown that complexes **1–3** obtain excellent double-carrier transport ability with the lowest unoccupied molecular orbital (LUMO) energy levels around 3.0 eV and the highest occupied molecular orbital (HOMO) energy levels around 5.3 eV. To the best of our knowledge, this is the best result for the frontier orbital energy levels of electroluminescent Eu^{III} complexes.

Furthermore, the complexes unexpectedly exhibited an amorphous state and extraordinarily low self-quenching. Stable red emissions from the single-layer and four-layer OLEDs based on pure complexes **1–3** were demonstrated. The maximum brightness of the single-layer device based on **2** was 59 cd m^{-2} . We believe that this is the best performance from single-layer devices based on pure Eu^{III} complexes. Both of the four-layer devices based on **1** and **2** had a maximum brightness of more than 1000 cd m^{-2} , turn-on voltages lower than 5 V, external quantum yields of more than 3%, and excellent spectral stability.

Results and Discussion

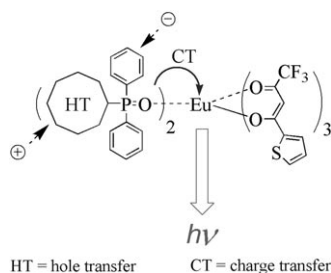
Design and synthesis of the functional single-coordinate phosphine oxide ligands: On account of the volume effect mentioned above, we thought that designing double-carrier-transport neutral ligands with the most compact structure would be very significant for comparison. In our former work, the phosphine oxide ligands exhibited very strong modification inertia. This advantage gave us a routine to design double-carrier-transport neutral ligands based on phosphine oxide compounds with the simplest and most



Scheme 1. Synthetic route to TAPO, NaDAPO, and CPPO and their complexes $[\text{Eu}(\text{tapo})_2(\text{tta})_3]$ (1), $[\text{Eu}(\text{nadapo})_2(\text{tta})_3]$ (2), and $[\text{Eu}(\text{cpo})_2(\text{tta})_3]$ (3). HTTA: 2-thenoyltrifluoroacetone.

compact structure, which are the direct combinations of hole-transport moieties and TPPO moieties. These functional single-coordinate phosphine oxide ligands have the most compact structure, as TPPO here serves not only as the coordinating group but also as the electron-transport group and no buffer group was used between the hole-transport groups and coordinating TPPO. Their compact structure can reduce the distance between the ligands and Eu^{III} ions, which would increase the efficiency of the Dexter energy

transfer in the corresponding Eu^{III} complexes. During the process of EL the relatively short distance between the ligands and Eu^{III} ions would make the ions more easily and efficiently excited through the process of charge-transfer excitation (Scheme 2). Simultaneously, because of their bipolar structure, hole and electron can be readily injected into these functional phosphine oxide ligands and their corresponding complexes. Compared with TPPO and its Eu^{III} complex, the hole-transport ability of the ligands and their



Scheme 2. Effect of the functional single-coordinate phosphine oxide ligands in their Eu^{III} complexes.

complexes is much improved, and a balance of the hole and electron injection and transport in the complexes can be expected.

These phosphine oxide ligands can be synthesized by a simple three-step process. Amines or carbazole first underwent the Ullmann reaction with 4-bromiodobenzene to yield the corresponding bromides. The bromides were then successively reacted with *n*-butyllithium, chlorodiphenylphosphine, and hydrogen peroxide to form the corresponding phosphine oxide ligands. These functional phosphine oxide ligands were characterized by NMR spectroscopy, mass spectrometry (MS), and elemental analysis. Their Eu^{III} complexes were synthesized according to a well-established procedure.^[26]

Optical properties: The UV/Vis absorbance and PL spectra of complexes **1–3** in dilute CH_2Cl_2 solutions ($1 \times 10^{-5} \text{ mol L}^{-1}$) and as the solids were measured (Figure 1). In solution, complexes **1** and **2** have similar UV/Vis characteristics with one main peak around 330 nm, originating from the neutral ligands TAPO and NaDAPO, and another shoulder peak at shorter wavelength contributed by the anionic ligand TTA and the neutral ligands, respectively; the main absorbance peak of **3** at 338.5 nm and a sharp

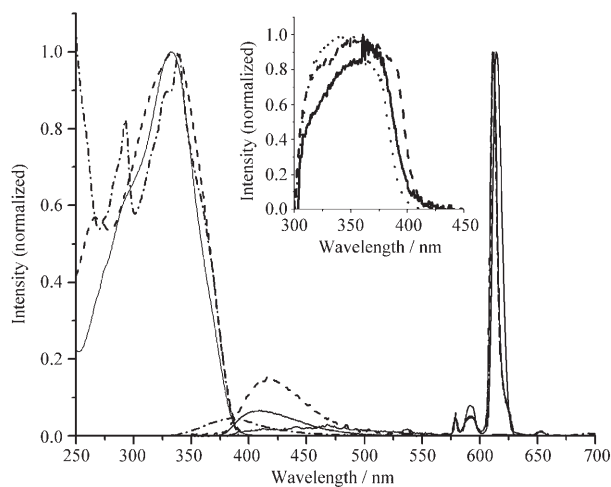


Figure 1. UV and PL spectra of **1–3** in CH_2Cl_2 solution and in the solid state (insert). —: **1**, ----: **2**,: **3**.

peak at 292.5 nm mainly originate from CPPO. In the solid, all of the complexes have a wide absorbance peak from 300 to 400 nm. In the PL spectra (excitation at 380 nm), besides the four main peaks at 579, 593, 611, and 653 nm, which are the characteristic emissions from Eu^{III} corresponding to $^5\text{D}_0\text{--}^7\text{F}_j$ ($j=0\text{--}3$) transitions, wide and much weaker peaks in the short-wavelength range are recognized as the emissions from TAPO, NaDAPO, or CPPO. Further studies of the PL spectra of **1** in different solvents (excitation at 360 nm) showed that with increasing polarity of the solvents, the increasing emission intensity of TAPO became stronger and the emissions from Eu^{III} were weakened markedly (Figure 2). This finding proved that the solvent effect should be one of the most important factors for this inefficient intramolecular energy transfer, which induces the visible emissions from TAPO, NaDAPO, and CPPO. The emission of TAPO was red-shifted about 10 nm in ethanol solution, which was induced by the protonic solvent effect on the $\pi\text{--}\pi^*$ transition of TAPO.

As single-coordinate ligands, the structures of complexes **1–3** are not rigid enough such that the small solvent molecules could enter the complexes, increase the distance between the phosphine oxide ligands and the Eu^{III} centre, and further reduce the Dexter energy-transfer efficiency. Due to their coordination ability, THF and ethanol amplified the solvent effect by entering the complexes as solvent ligands. However, the intensity of the short-wavelength emissions was much smaller than that of the emission from Eu^{III} when excited by an appropriate wavelength in CH_2Cl_2 , which means that only a small fraction of the energy of these neutral ligands is given out as their own emissions rather than transfers to Eu^{III} . Furthermore, in the solid state the emissions from these phosphine oxide ligands nearly disappear and the main emissions of complexes **1–3** are at 615 nm (Figure 1).

The relative PL quantum yields of complexes **1–3** were measured by using $[\text{Ru}(\text{bpy})_3\text{Cl}_2]$ as a standard (see Table 1). Compared with $[\text{Eu}(\text{tppo})_2(\text{tta})_3]$ (26.7%),^[21] the

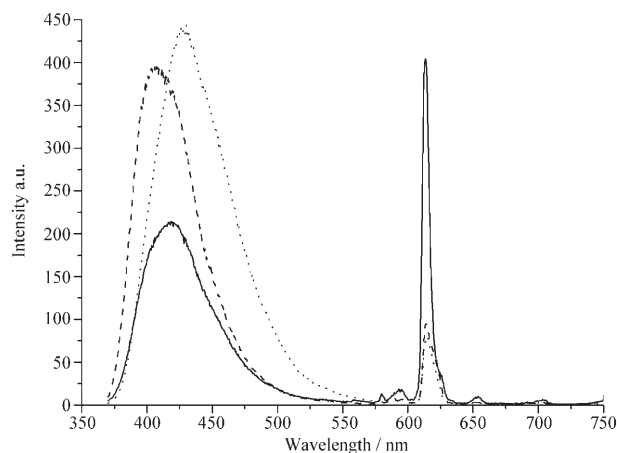


Figure 2. PL spectra of **1** in different solvents. —: in CH_2Cl_2 , ----: in THF,: in $\text{C}_2\text{H}_5\text{OH}$.

Table 1. The relative PL quantum yield (QY) of the complexes.

Complex	Absorption peak [nm]		PL emission peaks [nm]		Relative PL QY [%]
	CH ₂ Cl ₂	Film	CH ₂ Cl ₂	Film	
[Eu(tppo) ₂ (tta) ₃] ^[21]	265, 338	–	580, 617, 680	–	26.7
1	334	352	408, 579, 593, 611, 653	579, 592, 615	39.4
2	266, 335	364	414, 579, 593, 611, 653	579, 592, 615	36.1
3	293, 339	341	383, 579, 593, 611, 653	579, 593, 615	42.5

relative PL quantum yields of **1–3** are improved much more. It is shown that the introduction of chromophore groups, such as amines and carbazole, can improve the PL properties of the corresponding complexes. As steric effects induce a decrease of the intramolecular energy-transfer efficiency, the compact neutral ligands in **1–3** can limit this effect.

Intramolecular energy transfer in the complexes: The absorption and PL spectra of the ligands (TAPO, NaDAPO, CPPO, and TTA) were measured (Figure 3). There are overlaps between the emission peaks of these neutral ligands and the absorbance peak of TTA, which shows the possibility of energy transfer from the ligands to TTA.

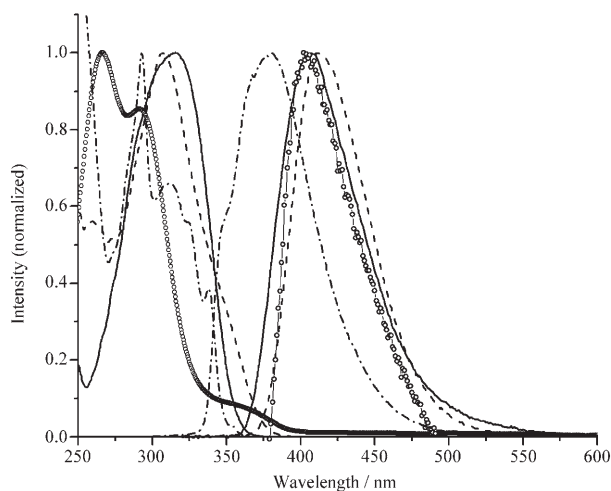


Figure 3. UV and PL spectra of the ligands TAPO, NaDAPO, CPPO, and TTA in CH₂Cl₂ solution. —: curves of TAPO, ----: curves of NaDAPO, -.-.: curves of CPPO, ○: curves of TTA.

The first triplet excited energy levels (T_1) of TAPO, NaDAPO, and CPPO were obtained by measuring the phosphorescence spectra of the gadolinium complexes based on these neutral ligands corresponding to their peak emission wavelengths (2.90 (428), 2.92 (425), and 2.84 eV (437 nm); Figure 4). The first singlet excited energy levels (S_1) of TAPO, NaDAPO, and CPPO are estimated by referencing their absorbance edges, which are 3.50 (354.5), 3.32 (373.5), and 3.54 eV (350 nm). For comparison, the singlet- and triplet-state energy levels are summarized in Table 2 and illustrated in Figure 5.

The energy absorbed by the neutral ligands can be transferred to the S_1 level of TTA, as all of the S_1 levels of these

neutral ligands are higher than that of TTA (Figure 5). Alternatively, compared with TPPO the introduction of the amines and carbazole as chromophore groups into phosphine oxide compounds remarkably reduces

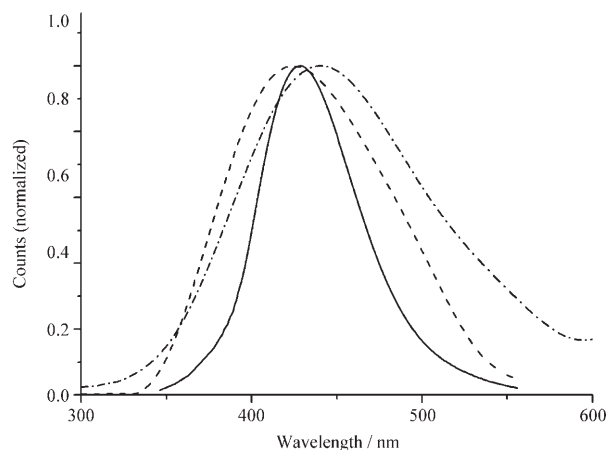


Figure 4. Smoothed phosphorescence spectra of the Gd^{III} complexes containing TAPO, NaDAPO, or CPPO. —: curve of [Gd(NO₃)₃(tapo)₂], ----: curve of [Gd(NO₃)₃(Nadapo)₂], -.-.: curve of [Gd(NO₃)₃(cpno)₂].

Table 2. The singlet- and triplet-state energy levels of ligands.

Ligand	S_1 energy level [eV]	T_1 energy level [eV]
TAPO	3.50	2.90
NaDAPO	3.32	2.92
CPPO	3.54	2.84
TPPO ^[22]	4.51	2.35
TTA ^[20]	3.12	2.35

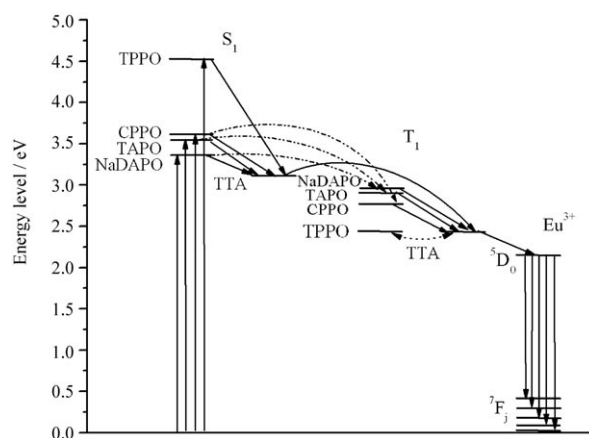


Figure 5. Schematic energy-level diagram and the energy-transfer process: S_1 , first excited singlet state; T_1 , first excited triplet state.

their S_1 levels. The degrees of reduction of the S_1 levels of TAPO and CPPO are equivalent, and because of the longer conjugated length of naphthalenyl moieties NaDAPO has the lowest S_1 level. In $[\text{Eu}(\text{tpo})_2(\text{tta})_3]$, the energy transfer from the S_1 level of TPPO to that of TTA is inefficient, as their energy gap is as large as 1.4 eV. Clearly, by modification with chromophore groups, the S_1 levels of TAPO, NaDAPO, and CPPO are reduced to fit that of TTA. In particular, for TAPO and CPPO the mezzo energy gaps of about 0.4 eV between their S_1 levels and that of TTA make the energy transfer between them more efficient. Notably, contrary to the reduction of their S_1 levels, the T_1 levels of TAPO, NaDAPO, and CPPO rise to positions between the S_1 and T_1 energy levels of TTA, and the energy gaps between the T_1 levels of these neutral ligands and that of TTA are about 0.5 eV. Without modification, TPPO has an equivalent T_1 energy level with TTA, which makes the positive energy transfer from the T_1 level of TPPO to that of TTA much more difficult in $[\text{Eu}(\text{tpo})_2(\text{tta})_3]$. However, because of their higher T_1 energy level the positive energy transfer from T_1 levels of TAPO, NaDAPO, and CPPO to that of TTA becomes preponderant, and the reverse energy transfer from TTA to neutral ligands is restrained. Consequently, most of the triplet excited energy of these neutral ligands can be efficiently transferred to 5D_0 of Eu^{III} through the T_1 level of TTA. In brief, modification with chromophore groups reduces the S_1 levels of TAPO, NaDAPO, and CPPO to fit that of TTA much more, which improves the intramolecular singlet energy transfer in the complexes and increases the S_1 energy-transfer efficiency. Simultaneously, because TAPO, NaDAPO, and CPPO have mezzo T_1 energy levels between the S_1 and T_1 energy levels of TTA, positive triplet energy transfer from these ligands to TTA becomes the main process. The triplet energy of the neutral ligands can be transferred to central ions more efficiently. These findings mean that the introduction of suitable chromophore groups can support phosphine oxide ligands with mezzo S_1 and T_1 energy levels and improve the intramolecular energy transfer in their Eu^{III} complexes.

Thermal properties: Thermogravimetric analysis (TGA) showed that the temperatures of the thermal decomposition (T_d) of complexes **1–3** are higher than 300 °C (334 °C for **1**, 312 °C for **2**, and 321 °C for **3**; Figure 6), which makes device fabrication by vacuum evaporation more feasible.

Notably, no melting point of complexes **1–3** was observed by cyclic differential scanning calorimetry (DSC) analysis (in every heating/cooling programme five cycles were scanned for each complex). This means that complexes **1–3** are amorphous, or at least it is difficult for them to crystallize. The formation of the amorphous states of these complexes is due to their single-coordinate phosphine oxide ligands, whose bigger volumes and degrees of freedom increase the volume of the complexes and decrease the intermolecular interaction. The stable amorphous states of complexes **1–3** are very important for increasing the morphological stability of the emitting-layer films in their

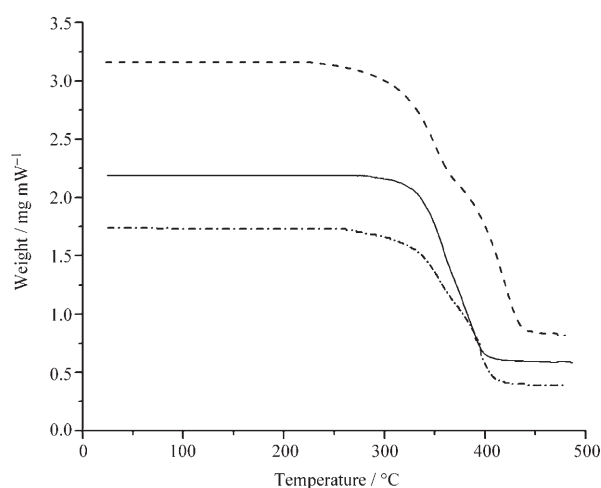


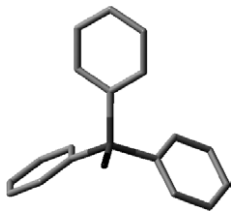
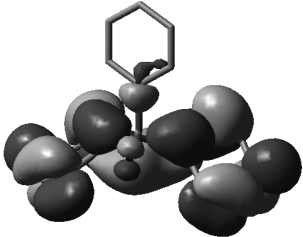
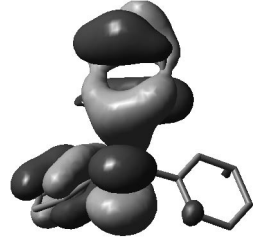
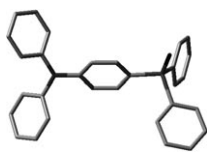
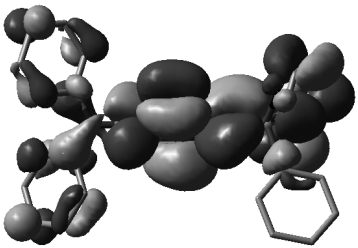
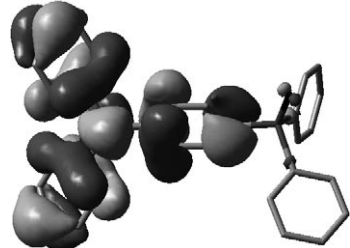
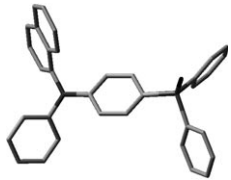
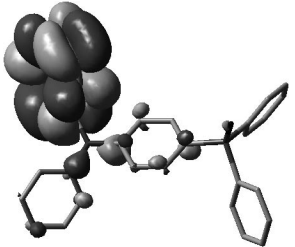
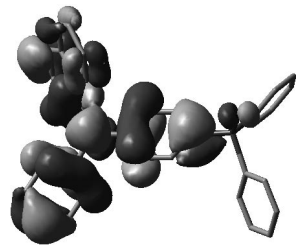
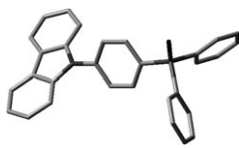
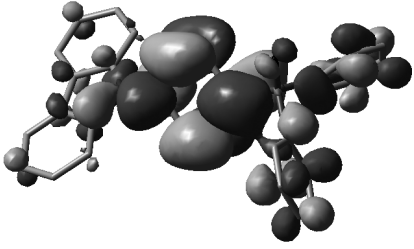
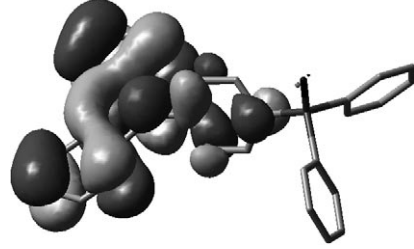
Figure 6. TGA curves of **1–3**. —: curve of **1**, ----: curve of **2**, -.-.: curve of **3**.

OLEDs during operation, which is significant for improving the lifetime of the devices. It is known that for electroluminescent Eu^{III} complexes, the triplet–triplet state (T–T) energy quenching highly decreases their EL efficiency. Thus, most of the electroluminescent Eu^{III} complexes were used as dopants in the OLED devices. However, the energy-transfer efficiency between host materials and Eu^{III} complexes was still not sufficient, and the phase separation during long-term operation would greatly decrease the performance of the devices. The amorphous state of **1–3** shows that the intermolecular interaction in these complexes is much weaker and the weaker interaction could decrease the T–T energy quenching. Therefore, the pure Eu^{III} complexes **1–3** can be used directly as emitting layers to support excellent EL performance.

Theoretical calculations: After modification with the hole-transport groups, the change in the carrier injection and transport ability of TAPO, NaDAPO, and CPPO was what we were interested in. It is known that the carrier injection and transport ability is relative to the frontier orbitals (the LUMO and HOMO) of the compounds. The geometry optimization and frontier orbital population analysis of TPPO, TAPO, NaDAPO, and CPPO were performed at the B3LYP/6-31G* level. All calculations were carried out by using the Gaussian 03 program package.

The electron clouds of the HOMO and LUMO energy levels of TPPO are mainly localized at the three phenyl groups (Table 3). However, in TAPO, NaDAPO, and CPPO the HOMO electron clouds are localized at the hole-transporting moieties (such as triphenylamine, naphthalenyl diphenylamine, and *N*-phenylcarbazole) and the LUMO electron clouds are mainly localized at the TPPO moieties except in NaDAPO, the LUMO electron cloud of which is mainly localized at the naphthalenyl moiety with a larger conjugated area. Compared with TPPO, the HOMO energy levels of TAPO, NaDAPO, and CPPO rise remarkably, the

Table 3. The calculated geometry, contours, and energy levels of the frontier orbitals.

Ligands	Geometry	LUMO energy orbital	HOMO energy orbital	LUMO [eV]	HOMO [eV]
TPPO				-0.844	-6.721
TAPO				-0.816	-5.143
NaDAPO				-1.224	-5.224
CPPO				-1.007	-5.442

LUMO energy levels of NaDAPO and CPPO fall substantially, and the LUMO energy level of TAPO is equivalent to that of TPPO. Both TAPO and CPPO exhibit the characteristic bipolar structure. It is clear that at the same time as improving their hole-injection ability by introducing hole-transport groups, TAPO, NaDAPO, and CPPO also have excellent electron-transport ability. With this double-carrier transport ability, these single-coordinate phosphine oxide ligands can greatly improve the relevant performance of their Eu^{III} complexes, possibly balance the carrier injection and transport in the complexes, and increase the EL efficiency of the OLEDs.

Electrochemical properties: The redox behavior of complexes **1–3** is of much interest as it can give information about the HOMOs and LUMOs of the complexes, which are considered to determine the carrier injection and transport ability. As they contain double-carrier-transporting

phosphine oxide ligands, a balanceable electron and hole injection and transport in complexes **1–3** was expected.

The electrochemical properties of complexes **1–3** were investigated by CV at room temperature in acetonitrile measured against an Ag/Ag⁺ (0.1M in acetonitrile) electrode (0.34 V versus saturated calomel electrode (SCE); Figure 7) and the data are listed in Table 4 for comparison. All of complexes **1–3** displayed a single, reversible, one-electron oxidation wave at 0.75, 0.78 or 1.32 V. Their onset potentials were 0.5, 0.551 and 0.948 V, respectively. According to the equation reported by de Leeuw et al.,^[23] $E_{\text{HOMO}} = (E_{\text{onset} \rightarrow \text{SCE}}^{\text{Oxy}} + 4.4 \text{ eV})$ and $E_{\text{LUMO}} = (E_{\text{onset} \rightarrow \text{SCE}}^{\text{Red}} + 4.4 \text{ eV})$. So the E_{HOMO} values of complexes **1–3** are about -5.24, -5.29, and -5.69 eV, respectively, which approach the HOMO energy level (-5.2 eV) of *N,N*-bis(α -naphthylphenyl)-4,4'-biphenyldiamine (NPB) or *N,N'*-diphenyl-*N,N'*-bis(3-methylphenyl)-1,1'-biphenyl-4,4'-diamine (TPD) (the materials usually used as hole-transport layer). It is clear that the HOMOs of com-

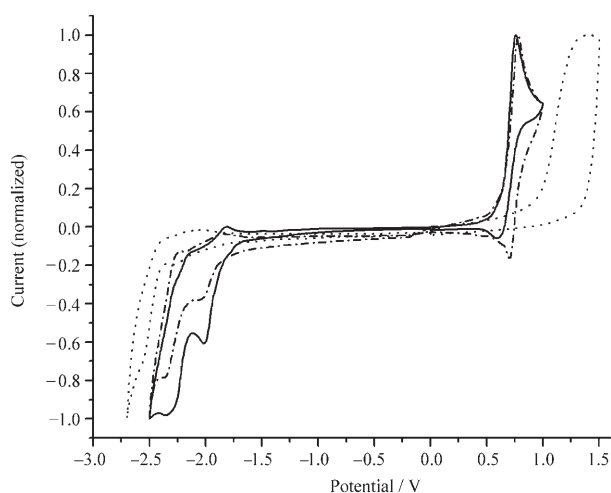


Figure 7. Cyclic voltammograms of **1–3**. —: curve of **1**, --: curve of **2**,: curve of **3**.

Table 4. Electrochemical properties of the complexes.

Complex	Voltage _{onset} ^{Oxy} [V] (E_{HOMO} [eV])	Voltage _{onset} ^{Red} [V] (E_{LUMO} [eV])
[Eu(phen)(tta) ₃] ^[24]	– (–6.3)	– (–3.1)
1	0.500 (–5.24)	–1.741 (–3.00)
2	0.551 (–5.29)	–1.660 (–3.08)
3	0.948 (–5.69)	–1.713 (–3.03)

plexes **1–3** have been increased high enough to improve their hole injection and transport ability by introducing hole-transport groups in the neutral ligands. The results show that the hole injection and transport ability of these complexes is as excellent as that of common hole-transporting materials. On the other hand, all the complexes **1–3** had two reversible, one-electron reduction waves (–2.02 and –2.35 V for **1**, –2.00 and –2.35 V for **2**, and –2.25, and –2.56 V for **3**) with onset potentials of –1.741, –1.660, and –1.713 V, respectively. According to the equation mentioned above, the E_{LUMO} values of the complexes are –3.00, –3.08, and –3.03 eV, which also approach the LUMO energy level of 2,9-dimethyl-4,7-diphenyl-1,10-phenanthroline (BCP; the material usually used as the electron-transporting hole-blocking layer).

To the best of our knowledge, among TTA-containing Eu^{III} complexes, the lowest LUMO and the highest HOMO energy levels reported so far are located at –3.1 and –6.3 eV for [Eu(phen)(tta)₃] with respect to the vacuum level.^[24] Compared with [Eu(phen)(tta)₃], the E_{HOMO} of **1**, for example, increases as much as 0.96 eV. This great improvement in hole injection and transport ability of complexes **1–3** is mainly caused by the functional phosphine oxide ligands modified by the hole-transport moieties. Simultaneously, with the contribution from the rest of the phosphine oxide moieties of the ligands, the complexes, the E_{LUMO} values of which are equivalent to that of [Eu(phen)(tta)₃], still have a very good electron injection and transport ability. With LUMOs and HOMOs fitting to the corre-

sponding carrier-transport layers (NPB and BCP), complexes **1–3** would have an excellent double-carrier injection and transport ability, which is very important for carrier-transport balance in emitting layers of OLEDs. It is proved that by taking advantage of the unique structure of phosphine oxide ligands, while at the same time preserving the good electron-transport ability of TPPO moieties, the introduction of hole-transport moieties in phosphine oxide ligands can greatly improve the hole-transport ability of the corresponding Eu^{III} complexes.

EL performance of OLEDs: Encouraged by the results of CV and other analyses, we studied the EL properties of complexes **1–3**. As mentioned above, the amorphous state of complexes **1–3** shown by DSC decreases the T–T quenching, which means that these complexes can be used as an emitting layer directly. Furthermore, their LUMOs and HOMOs that fit to the corresponding carrier-transport layers (NPB and BCP) support enough carrier-transport ability without using any host materials. Two types of OLED structure were designed and fabricated: single-layer devices **A–C** (based on complexes **1–3**, respectively) with the structure indium–tin oxide (ITO)/Eu^{III} complex (60 nm)/Mg_{0.9}Ag_{0.1} (200 nm)/Ag (80 nm); and four-layer devices **D–F** (based on complexes **1–3**, respectively) with structure ITO/NPB (30 nm)/Eu^{III} complex (40 nm)/BCP (30 nm)/tris(8-hydroxyquinoline)aluminum (Alq₃; 30 nm)/Mg_{0.9}Ag_{0.1} (200 nm)/Ag (80 nm). All of the devices gave the pure characteristic emission of the Eu^{III} ion at 616 nm corresponding to ⁵D₀–⁷F₂, which demonstrated the recombination of carriers in the emitting layers.

The brightness–current density–voltage curves of the single-layer devices are shown in Figure 8. The turn-on voltage of device **A** was 8.2 V at 1 cd m^{–2}, and its maximum brightness of 35 cd m^{–2} was achieved at 19.0 V with the current density of 161.2 mA cm^{–2}. Device **B** had a turn-on voltage at 8.2 V. The maximum brightness of device **B** was as high as 59 cd m^{–2} at 18.2 V with a current density of

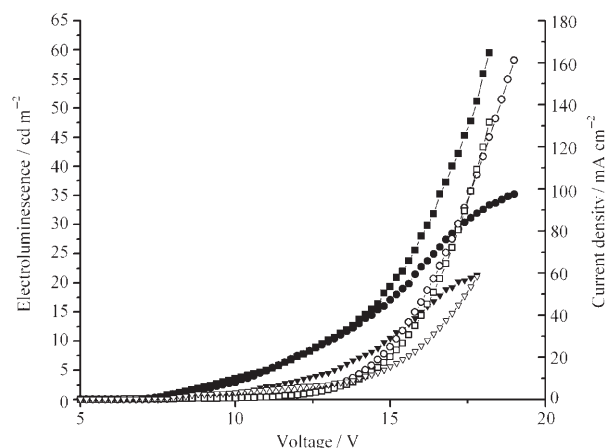


Figure 8. Brightness–current density–voltage curves of the single-layer devices **A–C**. Luminescence: ●: device **A**, ■: device **B**, ▼: device **C**; current density: ○: device **A**, □: device **B**, ▽: device **C**.

131.7 mA cm⁻². To the best of our knowledge, this is the highest luminescence from single-layer devices based on pure Eu^{III} complexes reported so far.^[9,12–14] Device **C** had a higher turn-on voltage of 10 V. Its maximum brightness of 21 cd m⁻² was achieved at 17.8 V and 58.4 mA cm⁻². Compared with [Eu(tppo)₂(tta)₃], the single-layer device of which had a brightness less than 1 cd m⁻², the performance of single-layer devices **A–C** was significantly improved. Notably, compared with the highest single-layer device brightness of 20 cd m⁻² reported by Huang and co-workers,^[14] the maximum brightness of devices **A** and **B** was remarkably increased, especially for device **B**, the highest brightness of which was nearly triple that of the largest value reported formerly.

The efficiencies of the devices at 10 cd m⁻² were calculated and are listed in Table 5. The efficiencies of devices **A** and **B** are much higher than that of device **C**. This trend

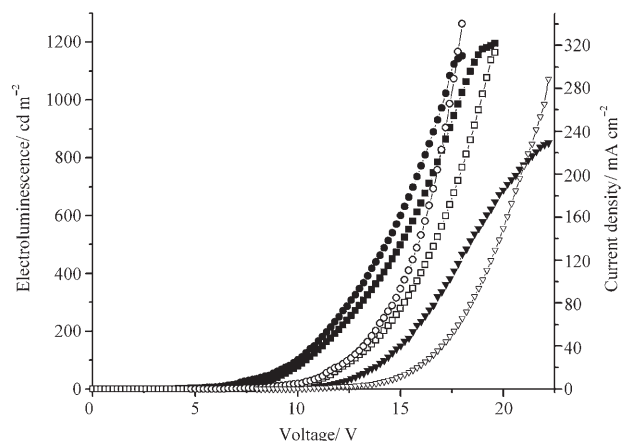


Figure 9. Brightness–current density–voltage curves of the four-layer devices **D–F**. Luminescence: ●: device **D**, ■: device **E**, ▼: device **F**; Current density: ○: device **D**, □: device **E**, ▽: device **F**.

Table 5. Efficiencies of devices **A–F**.

Device	Current efficiency [cd A ⁻¹]/voltage [V] (current density [mA cm ⁻²])		Power efficiency [lm W ⁻¹]/voltage [V] (current density [mA cm ⁻²])		External quantum yield [%]	
	Max.	100 cd m ⁻²	Max.	100 cd m ⁻²	Max.	100 cd m ⁻²
A	0.186/13 (5.33) ^[a]	–	0.045/13 (5.33) ^[a]	–	0.12 ^[a]	–
B	0.217/13 (4.66) ^[a]	–	0.052/13 (4.66) ^[a]	–	0.09 ^[a]	–
C	0.07/14.8 (14.1) ^[a]	–	0.015/14.8 (14.1) ^[a]	–	0.04 ^[a]	–
D	5.07/4.4 (0.021)	2.08/10.4 (4.82)	3.62/4.4 (0.021)	0.63/10.4 (4.82)	3.2	1.31
E	5.88/5.0 (0.032)	1.92/10.0 (5.24)	3.69/5.0 (0.032)	0.60/10.0 (5.24)	3.71	1.21
F	3.25/8.4 (0.028)	1.44/14.2 (6.92)	1.23/8.4 (0.028)	0.32/14.2 (6.92)	2.08	0.90

[a] At a brightness of 10 cd m⁻².

agrees with the variation of hole injection and transport ability of complexes **1–3** (**C** based on **3**, with the weakest hole injection and transport ability, exhibited the lowest efficiencies). It is demonstrated that through tuning the hole injection and transport ability of the complexes by introducing different hole-transport moieties, a balance of carrier transport can be achieved which leads to the great improvement of the EL performance of the complexes. The lower turn-on voltages and higher brightness of devices **A–C** show that complexes **1–3** have excellent and balanceable carrier-transport ability by themselves and much weaker self-quenching. Therefore, the four-layer devices were also fabricated by using pure complexes **1–3** as emitting layers directly. The carrier-transport layers were injected not only to enhance the carrier transport in devices but also to improve the interfaces between electrodes and the emitting complexes.

The brightness–current density–voltage curves of the four-layer devices **D–F** were measured (Figure 9). The turn-on voltage of device **D** was as low as 4.4 V at 1 cd m⁻², and its greatest brightness as high as 1195 cd m⁻² was achieved at 19.6 V with a current density of 313.26 mA cm⁻². Device **E** had a turn-on voltage at 4.8 V. The maximum brightness of device **E** was 1158 cd m⁻² at 18.0 V with the current density of 340.03 mA cm⁻². Device **F** could be turned on at 8.0 V with a maximum brightness of 852 cd m⁻² at 22.2 V with a current density of 288.48 mA cm⁻². As devices **D–F** were based on the pure Eu^{III} complexes with the same device

structure, their EL performance mainly originated from the relevant properties of the emitting complexes. It is clear that turn-on voltage is relative to the carrier injection and transport ability of the Eu^{III} complexes as emitting layers. The much lower turn-on voltages of devices **D** and **E** compared with **F** show the much easier carrier injection and transport in **1** and **2**.

As all three complexes have an equivalent electron injection and transport ability (demonstrated by CV analysis), the stronger hole injection and transport ability of **1** and **2** compared with **3** should be the main factor inducing this difference. Furthermore, the much larger maximum brightness of devices **D** and **E** compared with **F** shows that more holes can be injected into **1** and **2** at lower operating voltages and further recombined with electrons to form more excitons, which would originate from the more balanceable carrier injection and transport ability of **1** and **2** than **3**.

The efficiencies of devices **D–F** were calculated and the curves are shown in Figures 10 and 11. The data are listed in Table 5 for comparison. **D** and **E** showed very high current efficiencies of more than 5 cd A⁻¹ and an external quantum yield of more than 3% at very small current densities. At the practical luminescence of 100 cd m⁻², the current efficiencies and external quantum yield of **D** and **E** are still about 2 cd A⁻¹ and 1.2%, respectively. The brightness of over 1000 cd m⁻² and the high efficiencies at 100 cd m⁻² of the undoped devices indicate the very low self-quenching of **1** and **2**. This means that the much weaker intermolecular interaction and the amorphous state of **1** and **2** induced by the larger and freer functional single-coordinate phosphine oxide ligands can efficiently inhibit the self-quenching effect. At current densities less than 10 mA cm⁻², **D** and **E** had much higher efficiencies than **F**. This finding means that

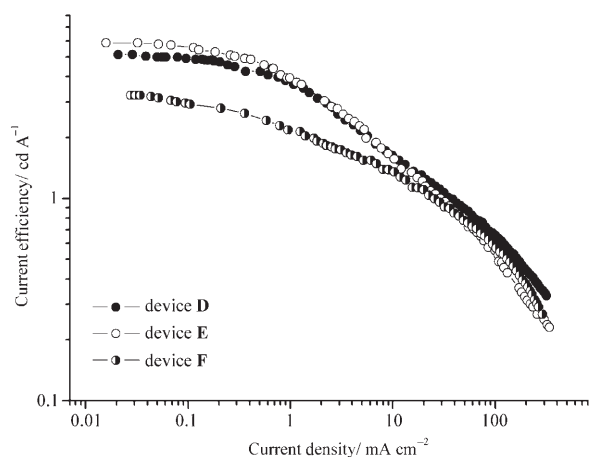


Figure 10. Current efficiency–current density curves of the four-layer devices **D–F**.

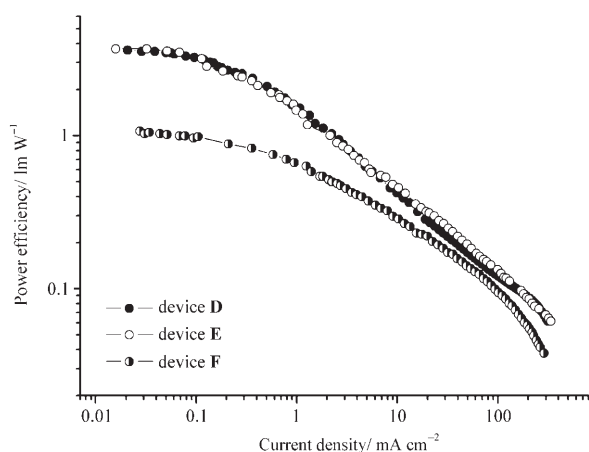


Figure 11. Power efficiency–current density curves of the four-layer devices **D–F**.

when the carrier density in the device is limited, the capability of capturing carriers of the complexes directly influences both the brightness and the efficiency of the devices, since the self-quenching effect is not evident at low exciton density. However, when the current density became more than 10 mA cm^{-2} , along with the current density increase the efficiencies of **D–F** decreased very rapidly. Notably, the current efficiency of **E** was reduced faster than those of **D** and **F** (Figure 10). The π – π stacking trend of the naphthalenyl group with a longer conjugated length in NaDAPO would enhance the intermolecular interaction in **2**, which should be the main factor that induces the worse self-quenching in **E**. Nevertheless, because of the stronger carrier injection and transport ability of **1** and **2**, **D** and **E** had lower operation voltages at the same current density compared with **F**, which made the power efficiencies of **D** and **E** constantly higher than that of **F**.

Table 6 shows recent representative work on electroluminescent functional Eu^{III} complexes. The EL performance of the single-layer and four-layer devices based on **2** compared

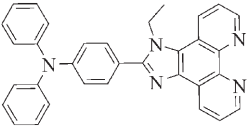
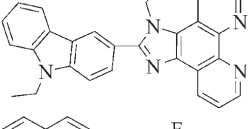
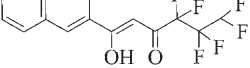
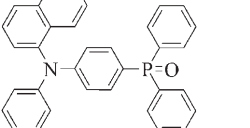
favorably with these results. The functional single-coordinate phosphine oxide ligands support the excellent EL properties of Eu^{III} complexes with a very simple structure, which should originate from the structure characteristic of phosphine oxide compounds and their special coordination mode.

The EL spectra of devices **D–F** show the characteristic emissions from Eu^{III} with the main peak at 616 nm (Figure 12). Devices **D** and **E** exhibited excellent spectral stability during the increase in operation voltage. However in the EL spectrum of **F**, the emission from Alq_3 at about 520 nm became more and more visible during voltage increase, which was also reported in previous work.^[5,14,25] According to the energy-level schemes in Figure 12, it is clear that in devices **D** and **E**, because of the higher HOMO energy levels of **1** and **2**, the hole cannot jump across energy gaps as big as $\approx 1.5 \text{ eV}$ to enter into Alq_3 even at breakdown voltages, so no emission from Alq_3 was observed. However, in **F** the lower HOMO energy level of **3** nearly halves the energy gap between hole-transporting NPB and hole-blocking BCP. The hole can make use of the HOMO energy level of **3** to cross the layer of BCP and enter into Alq_3 at higher voltages. This result proves that increasing the HOMO energy level of the Eu^{III} complexes can efficiently improve the EL efficiency by limiting holes in emitting layers, and enhances the spectral stability of the complexes.

Conclusion

Three functional single-coordinate phosphine oxide ligands with the most compact structure and their Eu^{III} complexes were designed and synthesized. Our investigations show that the introduction of hole-transport groups in single coordinate phosphine oxide ligands significantly improves the properties of their Eu^{III} complexes. The introduction of chromophore groups makes TAPO, NaDAPO, and CPPO obtain mezzo S_1 and T_1 energy levels, which fit those of TTA much more. Simultaneously, the ligands were designed with a structure that is the simplest and most compact possible in order to shorten the distance between ligands and Eu^{III} ions. The match of the excited energy levels and the compact structure of the complexes improve the intramolecular energy-transfer efficiency. On the other hand, the modification increases the volumes of the complexes, which reduces the intermolecular interaction and results in the amorphous phase and the extraordinarily low self-quenching of the complexes. The LUMO and HOMO energy levels of complexes **1–3** were tuned to fit the corresponding carrier-transport layer. The single-layer and four-layer OLEDs based on pure Eu^{III} complexes **1–3** had excellent EL performance, in which the single-layer device of **2** had the highest brightness of 59 cd m^{-2} reported so far and both of the four-layer devices based on **1** and **2** had a maximum brightness of more than 1000 cd m^{-2} , turn-on voltages lower than 5 V, external quantum yields of more than 3%, and excellent spectral stability. Compounds **1** and **2** are among the most

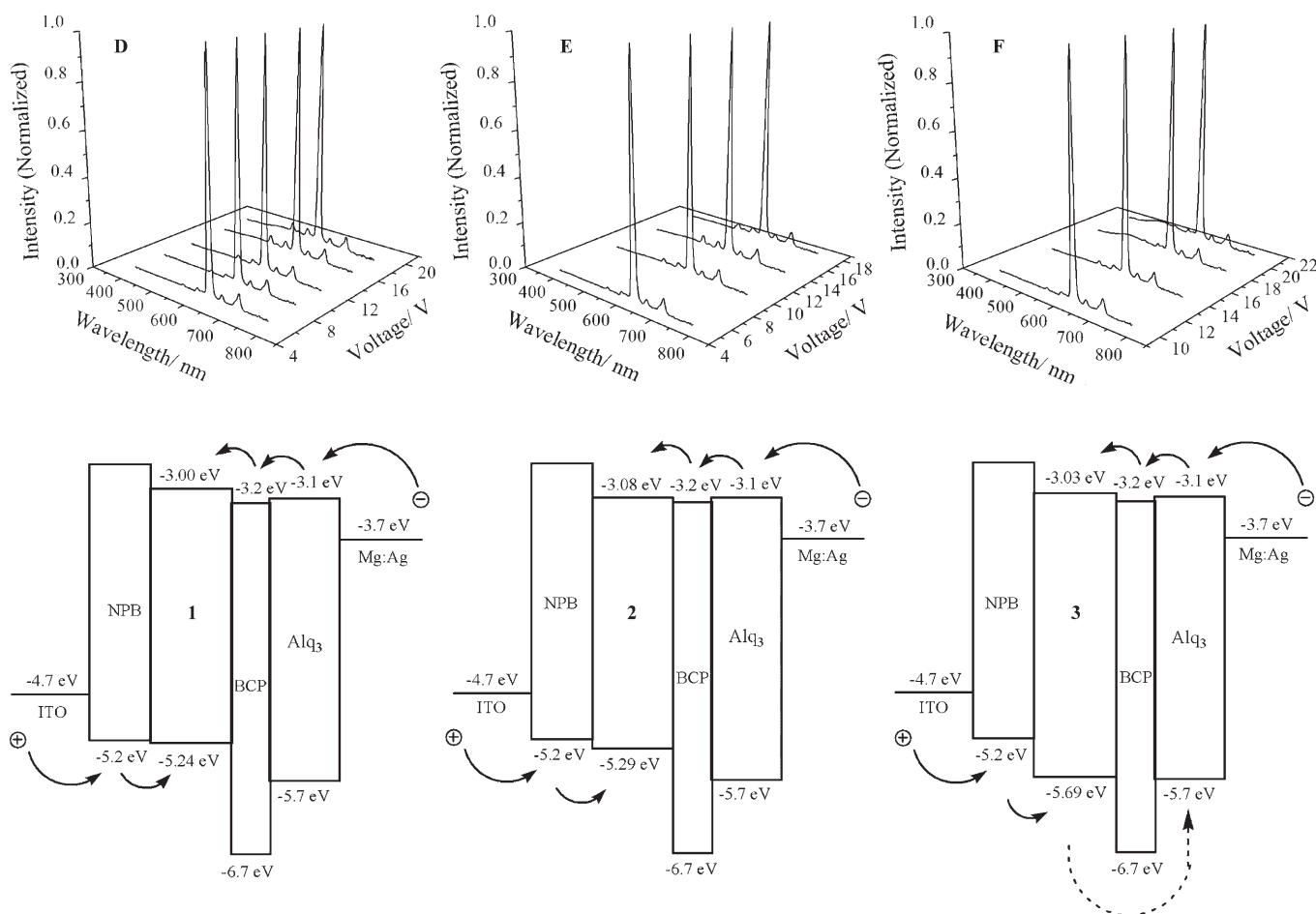
Table 6. Summary of the EL performance of the Eu^{III} complexes with functionalized ligands.

Ligand	Turn-on voltage (maximum brightness/voltage [V, cdm ⁻² /V])		Current efficiency [cd A ⁻¹]	Power efficiency [lm W ⁻¹]	Ref.
	Single-Layer Device	Multi-layer Device			
	8 (19/13.5)	6 (1305/16)	–	1.44	[13]
	7 (20/16)	5 (1500/16)	–	2.7	[14]
	–	5.7 (957/19.1)	4.14	2.28	[8]
	8.2 (59/18.2)	4.8 (1152/18)	5.88	3.69	this work

efficient Eu^{III} complexes. Our results demonstrate the further application of single-coordinate phosphine oxide ligands in high-performance electroluminescent Eu^{III} complexes by appropriate chemical modifications.

Experimental Section

Materials and instrumentation: All the reagents and solvents used for the synthesis of **1–3** were purchased from Aldrich and Acros. Alq₃, BCP, and NPB used for electroluminescent device fabrication were purchased from Lumtec Corporation. All the reagents were used without further purification. ¹H NMR spectra were recorded by using a Varian Mercury Plus 400NB spectrometer relative to tetramethylsilane (TMS) as internal standard. Molecular masses were determined by a Shimadzu laser desorption/ionization

Figure 12. EL spectra and energy-level schemes of devices **D–F**.

time-of-flight (LDI-TOF) mass spectrometer or a Shimadzu GCMS-QP2010 Plus instrument equipped with a DB-5 column. Elemental analyses were performed on a Vario EL III elemental analyzer. TGA and DSC were performed on Shimadzu DTG-60A and DSC-60A thermal analyzers under a nitrogen atmosphere at a heating rate of $10^{\circ}\text{Cmin}^{-1}$. Absorption and PL emission spectra of the target compounds were measured in dichloromethane with a Shimadzu UV-3150 spectrophotometer and a Shimadzu RF-5301PC spectrophotometer, respectively. Phosphorescence spectra were measured in dichloromethane by using an Edinburgh FLS 920 fluorescence spectrophotometer at 77 K with cooling by liquid nitrogen.

(4-Bromophenyl)diphenylamine: Potassium carbonate (1.95 g, 14.1 mmol), copper sulfate pentahydrate (0.176 g, 0.705 mmol), 4-iodobromobenzene (7.64 g, 26.0 mmol), and diphenylamine (2.40 g, 14.1 mmol) were added to a 100 mL two-necked round-bottomed flask. The mixture was heated to 220°C for 15 h. Water (10 mL) was added to stop the reaction, and then the mixture was extracted with dichloromethane (3×30 mL). The organic layer was dried with MgSO_4 . The solvent was removed in vacuo and the residue was purified by flash column chromatography by using petroleum ether as the eluent. Small white crystals; yield: 2.92 g of (62%); $^1\text{H NMR}$ (CDCl_3 , 400 MHz): $\delta = 7.32$ (d, $J = 8.0$ Hz, 2H), 7.23–7.27 (m, 4H), 6.62 (t, $J = 8.0$ Hz, 2H), 7.01–7.08 (m, 6H), 6.94 ppm (d, $J = 8.0$ Hz, 2H); GCMS: m/z (%): 323 (100) [M^+].

(4-Diphenylaminophenyl)diphenylphosphine oxide (TAPO): (4-Bromophenyl)diphenylamine (324 mg, 1 mmol) was dissolved in absolute ether (10 mL) and lithium salts were formed with 1.6 M *n*BuLi/hexane solution (0.75 mL, 1.2 mmol) at 0°C for 1 h. Then diphenylphosphine chloride (0.23 mL, 1.3 mmol) was added dropwise at 0°C . The mixture was reacted at 0°C for 1 h and then at room temperature overnight. The phosphine compound (4-diphenylaminophenyl)diphenylphosphine was obtained and purified by flash column chromatography by using dichloromethane as the eluent. Yellow powder; yield: 300 mg of (70%); $^1\text{H NMR}$ (CDCl_3 , 400 MHz): $\delta = 7.30$ –7.38 (m, 8H), 7.21–7.30 (m, 4H), 6.97–7.20 ppm (m, 10H); LDI-TOF-MS: m/z (%): 429 (100) [M^+]; elemental analysis calcd (%) for $\text{C}_{30}\text{H}_{24}\text{NP}$: C 83.89, H 5.63, N 3.26; found: C 83.58, H 5.51, N 3.09. The phosphine (429 mg, 1 mmol) was dissolved in 1,4-dioxane and sufficient dilute sulfuric acid was added to protect the N atoms. Then the phosphine was oxidized by 30% hydrogen peroxide (1.1 mmol) for 4 h to form the ligand TAPO. Straw-yellow powder; yield: 441 mg (99%); $^1\text{H NMR}$ (400 MHz, CDCl_3): $\delta = 7.65$ –7.76 (m, 4H), 7.37–7.58 (m, 9H), 7.24–7.35 (m, 4H), 7.07–7.18 (m, 5H), 6.97–7.06 ppm (q, $J_{\text{H-H}} = 8.8$, $J_{\text{P-H}} = 2.4$ Hz, 2H); LDI-TOF-MS: m/z (%): 445 (100) [M^+]; elemental analysis calcd (%) for $\text{C}_{30}\text{H}_{24}\text{NOP}$: C 80.88, H 5.43, N 3.14, O 3.59; found: C 80.37, H 5.77, N 3.06, O 3.73.

(4-Bromophenyl)naphthalen-1-yl-phenylamine: (4-Bromophenyl)naphthalen-1-yl-phenylamine was prepared from naphthalen-1-yl-phenylamine by following the same synthetic procedure as that for (4-bromophenyl)diphenylamine. White powder; yield: 71%; $^1\text{H NMR}$ (CDCl_3): $\delta = 7.95$ –8.01 (d, $J = 8.0$ Hz, 1H), 7.86–7.93 (d, $J = 8.0$ Hz, 1H), 7.76–7.83 (d, $J = 8.4$ Hz, 1H), 7.46–7.59 (m, 2H), 7.39–7.46 (t, $J = 7.4$ Hz, 1H), 7.30–7.38 (m, 3H), 7.28–7.20 (t, $J = 8.0$ Hz, 2H), 7.02–6.94 (m, 3H), 6.81–6.72 ppm (d, $J = 8.8$ Hz, 2H); GCMS: m/z (%): 373 (100) [M^+].

(4-Naphthalen-1-yl-phenylaminophenyl)diphenylphosphine oxide (NaDAPO): NaDAPO was prepared from (4-bromophenyl)naphthalen-1-yl-phenylamine by following the same two-step synthetic procedure as that for TAPO. Pale-yellow powder; yield 43%; $^1\text{H NMR}$ (CDCl_3): $\delta = 7.85$ –7.93 (brs, 2H), 7.78–7.84 (d, $J = 8.0$ Hz, 1H), 7.62–7.76 (m, 5H), 7.31–7.61 (m, 14H), 7.21–7.30 (m, 2H), 7.15–7.21 ppm (d, $J = 8.0$ Hz, 2H); LDI-TOF-MS: m/z (%): 495 (100) [M^+]; elemental analysis calcd (%) for $\text{C}_{34}\text{H}_{26}\text{NOP}$: C 82.41, H 5.29, N 2.83, O 3.23; found: C 82.06, H 5.77, N 2.80, O 3.48.

N-(4-Bromophenyl)carbazole: N-(4-Bromophenyl)carbazole was prepared from carbazole by following the same synthetic procedure as that for (4-bromophenyl)diphenylamine. White powder; Yield: 77%; $^1\text{H NMR}$ (CDCl_3): $\delta = 8.10$ –8.18 (d, $J = 8.0$ Hz, 2H), 7.69–7.75 (d, $J = 8.4$ Hz, 2H), 7.34–7.49 (m, 6H), 7.26–7.32 ppm (t, $J = 6.8$ Hz, 2H); GCMS: m/z (%): 321 (100) [M^+].

9-[4-(Diphenylphosphinyl)phenyl]-9H-carbazole (CPPO): CPPO was prepared from 9-(4-bromophenyl)-9H-carbazole in a yield of 53% as a white powder. $^1\text{H NMR}$ (CDCl_3): $\delta = 8.12$ –8.17 (d, $J = 7.6$ Hz, 2H), 7.86–7.95 (t, $J = 10.0$ Hz, 2H), 7.69–7.85 (m, 6H), 7.46–7.64 (m, 8H), 7.39–7.46 (t, $J = 7.6$ Hz, 2H), 7.28–7.36 ppm (q, $J_{\text{H-H}} = 10.0$ Hz, $J_{\text{P-H}} = 6.8$ Hz, 2H); LDI-TOF-MS: m/z (%): 443 (100) [M^+]; elemental analysis calcd (%) for $\text{C}_{30}\text{H}_{22}\text{NOP}$: C 81.25, H 5.00, N 3.16, O 3.61; found: C 81.65, H 4.88, N 3.57, O 4.00.

General procedure of complexation: The complexes were prepared according to well-established protocols.^[26] 2-Thenoyltrifluoroacetone (HTTA; 672.7 mg, 3 mmol) was dissolved in ethanol, and NaOH (120 mg, 3 mmol) in aqueous solution (2 M) was added to remove the H^+ in the TTA molecule. Then $\text{EuCl}_3 \cdot 6\text{H}_2\text{O}$ (370.1 mg, 1 mmol) in aqueous solution was added dropwise, the mixture was stirred at 60°C for 30 min, TAPO (890.0 mg, 2 mmol; or 990.0 mg of NaDAPO, or 886.0 mg of CPPO) in ethanol was added dropwise, and the mixture was stirred at 60°C for 4 h to afford the complexes 1–3. Purification was accomplished by precipitation from concentrated ethanol and water solution.

[Eu(tapo)₂(tta)₃] (1): Pale-yellow powder; yield 73%; $^1\text{H NMR}$ (CDCl_3 , 400 MHz): $\delta = 7.56$ –7.77 (brs, 16H; Ph–H), 7.22–7.36 (m, 14H; Ph–H), 7.13–7.22 (m, 14H; Ph–H), 7.05–7.12 (t, $J = 7.6$ Hz, 4H; Ph–H), 6.75–6.82 (d, 3H, $J = 4.8$ Hz; Th–H), 6.40–6.47 (t, 3H, $J = 4.4$ Hz; Th–H), 6.10–6.18 (d, 3H, $J = 2.8$ Hz; Th–H), 4.04 ppm (s, 3H; COCHCO); elemental analysis calcd (%) for $\text{C}_{84}\text{H}_{60}\text{EuF}_9\text{N}_2\text{O}_8\text{P}_2\text{S}_2$: C 59.12, H 3.54, Eu 8.91, N 1.64, O 7.50, S 5.64; found: C 59.01, H 3.685, Eu 9.14, N 1.408, O 7.14, S 5.80.

[Eu(nadapo)₂(tta)₃] (2): Pale-yellow powder; yield 62%; $^1\text{H NMR}$ (CDCl_3): $\delta = 7.90$ –7.98 (d, $J = 8.4$ Hz, 4H), 7.86–7.90 (d, $J = 8.4$ Hz, 4H), 7.77–7.83 (d, $J = 8.0$ Hz, 4H), 7.52–7.73 (brs, 16H), 7.43–7.50 (m, 7H), 7.33–7.41 (m, 6H), 7.15–7.24 (m, 11H), 6.72–6.80 (d, $J = 4.4$ Hz, 3H), 6.36–6.44 (t, $J = 4.0$ Hz, 3H), 6.06–6.12 (d, $J = 2.4$ Hz, 3H), 4.22 ppm (s, 3H); elemental analysis calcd (%) for $\text{C}_{92}\text{H}_{68}\text{EuF}_9\text{N}_2\text{O}_8\text{P}_2\text{S}_2$: C 61.16, H 3.57, Eu 8.41, N 1.55, O 7.08, S 5.32; found: C 61.35, H 3.69, Eu 8.87, N 1.54, O 7.12, S 5.34.

[Eu(cpapo)₂(tta)₃] (3): Pinkish white powder; yield 74%; $^1\text{H NMR}$ (CDCl_3): $\delta = 7.18$ –8.26 (m, 44H), 6.55–6.82 (brs, 3H), 6.12–6.33 (brs, 3H), 5.56–5.76 (brs, 3H), 4.12 ppm (s, 3H); elemental analysis calcd (%) for $\text{C}_{98}\text{H}_{56}\text{EuF}_9\text{N}_2\text{O}_8\text{P}_2\text{S}_2$: C 59.26, H 3.32, Eu 8.93, N 1.65, O 7.52, S 5.65; found: C 59.45, H 3.34, Eu 9.01, N 1.79, O 7.86, S 5.52.

General procedure for the preparation of gadolinium complexes: For triplet energy level measurement, gadolinium complexes comprising TAPO, NaDAPO, or CPPO without TTA were also synthesized.^[22] The phosphine oxide ligand (1 mmol) was dissolved in ethanol (15 mL). [$\text{Gd}(\text{H}_2\text{O})_6(\text{NO}_3)_3$] (0.5 mmol) in water (0.1 mL) was added to the solution dropwise with stirring and the mixture was heated to reflux for 2 h. The gadolinium complexes were recrystallized from concentrated methanol/water mixed solvent.

[Gd(NO₃)₃(tapo)₂]: White powder; elemental analysis calcd (%) for $\text{C}_{60}\text{H}_{48}\text{GdN}_3\text{O}_{11}\text{P}_2$: C 58.39, H 3.92, N 5.67, O 14.26; found: C 58.53, H 3.88, N 5.57, O 14.63.

[Gd(nadapo)₂(NO₃)₃]: White powder; elemental analysis calcd (%) for $\text{C}_{68}\text{H}_{52}\text{GdN}_3\text{O}_{11}\text{P}_2$: C 61.21, H 3.93, N 5.25, O 13.19; found: C 61.47, H 3.92, N 5.11, O 13.25.

[Gd(cpapo)₂(NO₃)₃]: White powder; elemental analysis calcd (%) for $\text{C}_{60}\text{H}_{44}\text{GdN}_3\text{O}_{11}\text{P}_2$: C 58.58, H 3.61, N 5.69, O 14.31; found: C 58.78, H 3.50, N 5.45, O 14.53.

Fabrication and testing of OLEDs: Single-layer and four-layer OLEDs were fabricated by vacuum deposition with the configurations ITO/Eu^{III} complex (60 nm)/Mg_{0.9}Ag_{0.1} (200 nm)/Ag (80 nm) and ITO/NPB (30 nm)/Eu^{III} complex (40 nm)/BCP (30 nm)/Alq₃ (30 nm)/Mg_{0.9}Ag_{0.1} (200 nm)/Ag (80 nm), in which NPB is the hole-transporting layer, BCP is the electron-transporting/hole-blocking layer, Alq₃ is the electron-transporting layer, and ITO and MgAg were used as the anode and cathode, respectively.^[27] Before loading into a deposition chamber, the ITO substrate was cleaned with detergents and deionized water, dried in an oven at 120°C for 4 h, and treated with UV/ozone for 25 min. Devices were fabricated by evaporating organic layers at a rate of 0.1 – 0.3 nm s⁻¹ onto the ITO substrate sequentially at a pressure below 1×10^{-6} mbar. A layer of

MgAg 200 nm in thickness was deposited on the Alq₃ layer at a rate of 0.4 nm s⁻¹ to improve electron injection. Finally, an 80 nm-thick layer of Ag was deposited at a rate of 0.6 nm s⁻¹ as the cathode. The emission area of the devices was 0.12 cm², as determined by the overlap area of the anode and cathode. The EL spectra and current–voltage–luminance characteristics were measured with a Spectrascan PR 650 photometer and a computer-controlled dc power supply under ambient conditions.

Acknowledgements

This work was financially supported by the National Natural Science Foundation of China under grants 60325412, 90406021, and 50428303. Helpful discussions with Professor C.-H. Huang, Professor F.-Y. Li, Dr. R.-F. Chen, Dr. S.-J. Liu and Dr. Q. Zhao are highly appreciated.

- [1] J. Kido, Y. Okamoto, *Chem. Rev.* **2002**, *102*, 2357–2368.
- [2] M. D. McGehee, T. Bergstedt, C. Zhang, A. P. Saab, M. B. O'Regan, G. C. Bazan, V. I. Srdanov, A. J. Heeger, *Adv. Mater.* **1999**, *11*, 1349–1354.
- [3] L. Huang, K.-Z. Wang, C.-H. Huang, F.-Y. Li, Y.-Y. Huang, *J. Mater. Chem.* **2001**, *11*, 790–793.
- [4] T. Ohmori, H. Kajii, T. Sawatani, H. Ueta, K. Yoshino, *Thin Solid Films* **2001**, *393*, 407–411.
- [5] P.-P. Sun, J.-P. Duan, H.-T. Shih, C.-H. Cheng, *Appl. Phys. Lett.* **2002**, *81*, 792–794.
- [6] P.-P. Sun, J.-P. Duan, J.-J. Lih, C.-H. Cheng, *Adv. Funct. Mater.* **2003**, *13*, 683–691.
- [7] X.-H. Zhu, L.-H. Wang, J.-R. Wang, W. Huang, J.-F. Fang, D.-G. Ma, *J. Mater. Chem.* **2004**, *14*, 2732–2733.
- [8] J. Yu, L. Zhou, H. Zhang, Y. Zheng, H. Li, R. Deng, Z. Peng, Z. Li, *Inorg. Chem.* **2005**, *44*, 1611–1618.
- [9] M. R. Robinson, M. B. O'Regan, G. C. Bazan, *Chem. Commun.* **2000**, 1645–1646.
- [10] R. Reyes, E. N. Hering, M. Cremona, C. F. B. da Silva, H. F. Brito, C. A. Achete, *Thin Solid Films* **2002**, *420–421*, 23–29.
- [11] X.-C. Gao, H. Cao, C.-H. Huang, S. Umitani, G.-Q. Chen, P. Jiang, *Synth. Met.* **1999**, *99*, 127–132.
- [12] Z. Bian, D. Gao, K. Wang, L. Jin, C. Huang, *Thin Solid Films* **2004**, *460*, 237–241.
- [13] M. Sun, H. Xin, K. Wang, Y. Zhang, L. Jin, C. Huang, *Chem. Commun.* **2003**, 702–703.
- [14] H. Xin, F. Y. Li, M. Guan, C. H. Huang, M. Sun, K. Z. Wang, Y. A. Zhang, L. P. Jin, *J. Appl. Phys.* **2003**, *94*, 4729–4731.
- [15] H. Xin, M. Sun, K. Wang, Y. Zhang, L. Jin, C. Huang, *Chem. Phys. Lett.* **2004**, *388*, 55–57.
- [16] D. L. Dexter, *J. Chem. Phys.* **1953**, *21*, 836–850.
- [17] G. A. Crosby, R. E. Whan, R. M. Alire, *J. Chem. Phys.* **1961**, *34*, 743–748.
- [18] J. Wang, R. Wang, J. Yang, Z. Zheng, M. D. Carducci, T. Cayou, *J. Am. Chem. Soc.* **2001**, *123*, 6179–6180.
- [19] Y. J. Fu, T. K. S. Wong, Y. K. Yan, X. Hu, *J. Alloys Compd.* **2003**, *358*, 235–244.
- [20] H. Xu, L. Wang, X. Zhu, K. Yin, G. Zhong, X. Hou, W. Huang, *J. Phys. Chem. B* **2006**, *110*, 3023–3029.
- [21] X. C. Gao, H. Cao, G. Q. Yao, C. H. Huang, L. Huang, *J. Rare Earth* **1999**, *17*, 170–174.
- [22] H. Xin, M. Shi, X. C. Gao, Y. Y. Huang, Z. Gong, D. Nie, H. Cao, Z. Bian, F. Li, C. Huang, *J. Phys. Chem. B* **2004**, *108*, 10796–10800.
- [23] D. M. de Leeuw, M. M. J. Simenon, A. R. Brown, R. E. F. Einerhand, *Synth. Met.* **1997**, *87*, 53–59.
- [24] Y. Ohmori, H. Kajii, T. Sawatani, H. Ueta, K. Yoshino, *Thin Solid Films* **2001**, *393*, 407–411.
- [25] J. Kido, H. Hayase, K. Hongawa, K. Nagai, K. Okuyama, *Appl. Phys. Lett.* **1994**, *65*, 2124–2126.
- [26] L. R. Melby, N. J. Rose, E. Abramson, J. C. Caris, *J. Am. Chem. Soc.* **1964**, *86*, 5117–5125.
- [27] J. F. Fang, D. G. Ma, *Appl. Phys. Lett.* **2003**, *83*, 4041–4043.

Received: May 4, 2007
Published online: October 4, 2007